JEE Journal of Ecological Engineering

Journal of Ecological Engineering, 2026, 27(2), 424–439
https://doi.org/10.12911/22998993/211728
ISSN 2299–8993, License CC-BY 4.0

Received: 2025.09.23
Accepted: 2025.12.15
Published: 2026.01.15

Estimating vehicular emissions on a main arterial road in Arar, Saudi Arabia: Insights for sustainable urban mobility

Tariq Alqubaysi[1]

[1] Department of Civil Engineering, College of Engineering, Northern Border University, Arar, 73222, Saudi Arabia
E-mail: tariq.alqubaysi@nbu.edu.sa

ABSTRACT

Rapid motorization in Saudi Arabia's secondary cities is intensifying concerns about local air quality, yet empirical, corridor-scale emission data remain scarce. This study integrates high-resolution traffic counts with regionally calibrated emission factors to characterize on-road pollutant loads along two arterial segments in Arar: (i) a free-flow highway section (Point A) and (ii) an urban, signal-controlled intersection (Point B). Vehicle volumes and classifications were recorded at 1-h resolution over seven consecutive days using MetroCount pneumatic sensors, capturing 53,749 and 55,116 vehicles at Points A and B, respectively. Baseline emission factors were derived from COPERT-6 and MOVES-5 models; to reflect local fleet age, fuel sulphury content and ambient temperatures, factors were uplifted by +15% for light-duty vehicles and +10–12% for heavy-duty vehicles. Despite similar traffic volumes, congestion at Point B markedly elevated pollutant intensities. Average weekday peak-hour speeds fell to 44.1 km/h for passenger cars and 29.9 km/h for heavy trucks, compared with 53.4 km/h and 42.7 km/h at Point A. Consequently, Point B exhibited 75% higher heavy-truck CO_2 emissions (1.27×10^6 g/day/km) and increases of 75% and 74% in NO_x (1 245 g/day/km) and $PM_{2.5}$ (16.4 g/day/km), respectively, relative to Point A. Although heavy-duty vehicles comprised less than 7% of the fleet, they accounted for ≈ 50% of corridor-wide NO_x and $PM_{2.5}$. A review of mitigation strategies suggests that restoring average speeds above 50 km/h or rerouting Euro VI-compliant trucks could reduce corridor $PM_{2.5}$ by ~20%. The findings reveal the main determinants of urban emission hotspots along the two principal arterial roads of mid-sized cities such as Arar. The insights from this study can support decision-makers in formulating medium- and long-term urban mitigation strategies to address the increasing roadside exposure in rapidly urbanizing Middle Eastern cities.

Keywords: traffic-related emissions, traffic counts, heavy-duty vehicles, adjusted emission factors, signalized intersection, Arar, Saudi Arabia.

INTRODUCTION

Urbanization has catalyzed unprecedented growth in vehicular traffic, positioning the transportation sector as a leading contributor to global air pollution and climate change. Urban roads are the vector for pollutants spreading, including aerosols (Piotrowicz and Polednik, 2019). Vehicles account for 20–30% of urban nitrogen oxide (NOx) emissions (vizen, 2025) and 15% of global CO_2 emissions (US EPA, 2016), exacerbating respiratory illnesses, acid rain, and global warming. While cities strive to meet air quality standards set by the World Health Organization (WHO) and the Paris Agreement, traditional emission inventories often rely on outdated or aggregated traffic data, such as annual vehicle kilometers traveled (VKT) or static fleet composition estimates. These methods lack the granularity to capture real-world driving patterns, such as stop-and-go traffic, speed fluctuations, and the growing prevalence of electric and hybrid vehicles. Consequently, policymakers face significant uncertainty in designing targeted interventions, from congestion pricing to low-emission zones.

This study addresses a critical research gap: the need for high-resolution, real-world traffic data to refine emission models and quantify the efficacy

of traffic management strategies. While automated traffic monitoring systems like MetroCount's RoadPod (Mararo et al., 2015; Segarra-Morales and Moreno, 2024),TIRTL sensors (Li et al., 2010) and Lidar and CCTV technologies (Ansariyar et al., 2024; Guan et al., 2023; Peppa et al., 2021) have revolutionized data collection, their integration with emission modeling frameworks remains underexplored. This paper proposes a novel framework to estimate emissions using MetroCount's vehicle classification, speed profiles, and axle-weight data, validated against established models like COPERT and MOVES. By correlating traffic dynamics with pollutant outputs, the study demonstrates how data-driven strategies, such as signal optimization and freight route management, can reduce emissions by up to 25% in urban corridors. The findings aim to empower cities to align traffic management with sustainability goals, offering a blueprint for cleaner, smarter mobility.

The evolution of traffic monitoring has transitioned from labor-intensive manual counts to automated systems capable of capturing high-resolution data. Early methods relied on human observers tallying vehicles at intersections, a process prone to human error and limited to short-term studies. The advent of inductive loop detectors in the 1960s enabled continuous counting but lacked vehicle classification capabilities. Modern systems, such as MetroCount's pneumatic tubes and Weigh-in-Motion (WIM) sensors (Adresi et al., 2024), classify vehicles by axle spacing and weight, while AI-powered cameras extract speed and acceleration data with high accuracy (Fathima et al., 2025; Gautam et al., 2025; N et al., 2023). For instance, a recent investigation (Segarra-Morales and Moreno, 2024) compared Bushnell radar gun and MetroCount MC5600 pneumatic counter measurements on an Ecuadorian rural road, finding radar gun readings averaged 48.127 km/h versus 43.579 km/h for the pneumatic counter, with optimal radar positioning determined at 80 meters distance after cosine effect corrections for the 3.5 m perpendicular offset. Similarly, LiDAR-equipped drones now supplement ground sensors in complex urban networks, offering 3D traffic flow visualization (Cherif et al., 2023; Gurung, 2025).

Vehicle emission estimation and prediction are inherently complex. However, models and techniques were extensively used and adapted for context-specific circumstances. Some emission models translate traffic data into pollutant outputs using factors derived from laboratory testing or on-road measurements. For instance, (Wei et al., 2021) investigated traffic pollution in Hong Kong using bus-mounted mobile sensors, revealing that NO and NO2 were predominantly from local sources (72–84% and 58–71% respectively) while PM2.5 and CO were mainly from background sources (55–65% and 73–79%), with highest pollutant concentrations clustering around tunnel entrances and congested areas, suggesting limitations in existing Low Emission Zone policies that focus solely on large buses. Other emission models are regulatory by nature. For instance, the COPERT model (COmputer Programme to calculate Emissions from Road Transport), widely adopted in Europe, estimates emissions based on vehicle categories, fuel types, and speed profiles In contrast, the U.S. Environmental Protection Agency's MOVES (Motor Vehicle Emission Simulator) incorporates localized traffic and meteorological data, while the IVE model (International Vehicle Emissions) focuses on developing countries with heterogeneous fleets (Kawsar et al., 2024; Saberiyansani et al., 2025; Xu et al., 2021). The COPERT, IV and MOVES models stem their successful implementation from their simplicity, scalability, and suitability for data-scarce regions. An alternative to above modeling tools, PEMS (Portable Emission Measurement System) and laboratory-based measurement systems provide real-world, on-road emission measurements (Giechaskiel et al., 2021; Matsuoka et al., 2025; Rymaniak et al., 2023). While PEMS delivers high-accuracy, vehicle-specific data ideal for validation and real-world compliance testing, its high cost and limited sample size contrast with MOVES and COPERT's ability to generate fleet-wide emission inventories and future scenarios, though these models rely on assumptions and average data that may not fully capture local driving conditions or vehicle-specific variations.

These latter models are widely used in urban planning and policy-making due to their reliance on readily available input data, such as traffic volume, vehicle classification, and average speeds, making them ideal for mid-sized cities like Arar, where detailed on-road emission measurements or advanced monitoring infrastructure may be limited. Emission factors, a cornerstone of these models, need to be calibrated using peer-reviewed studies in similar contexts to reflect local driving conditions and vehicle fleets. For instance, higher nitrogen oxide (NO_x) emission factors were assigned to diesel trucks, reflecting

their disproportionate contribution to NO_x pollution, while carbon monoxide (CO) spikes during idling are proved to occur at the signalized intersections. The calculation framework followed a standard gross emission formula: Emission (g/km) = Traffic Volume × Emission Factor × Average Speed Adjustment, where traffic volumes from automated count systems like Metrocount and camera-based systems were multiplied by pollutant-specific emission factors (differentiated by vehicle type) and adjusted for average speeds derived from observed driving patterns (e.g., stop-and-go delays).

The aim of the current study is to provide a case study of car emission estimation for a mid-size city experiencing rapid urban growth. Similar studies for Saudi cities, whichever medium or large, are up the author's best knowledge scarce or non-not yet conducted. The analysis focused on four key pollutants: carbon dioxide (CO_2), a major greenhouse gas; CO, indicative of incomplete combustion; NO_x, linked to respiratory illnesses; and particulate matter (PM), a critical pollutant affecting air quality and public health. By integrating localized data with established modeling frameworks, this approach balances computational efficiency with contextual accuracy, providing actionable insights for urban areas facing rapid traffic growth and limited emission monitoring capabilities.

For instance, this study examines vehicular emissions along a major arterial road in Arar, Saudi Arabia, where rapid urbanization and increasing vehicle usage have raised air quality concerns. The research primarily investigates the performance of gross emission estimation models for vehicular emissions, focusing on quantifying CO_2, CO, NO_x, and PM2.5 emissions at two strategic survey points: an entry point and a signalized intersection. The study's objectives include comparing the results with standard guidelines and analyzing the impacts of traffic volume. It also acknowledges limitations related to the gross estimation approach and data availability, particularly within the rapidly developing urban context of the study area

MATERIALS AND METHODS

Study area

Arar, a rapidly expanding urban center in northern Saudi Arabia, serves as the capital of the Northern Border Region and plays a pivotal role in regional trade and transportation due to its proximity to the Saudi-Iraqi border. With a current population of 219,079 and a projected annual growth rate of 1.7%, the city is expected to surpass 283,300 residents by 2030, driven by economic diversification and infrastructure development under Saudi Vision 2030. This growth has intensified urban sprawl, resulting in a distinct spatial divide: densely populated southern zones (150–200 people/km²), characterized by mixed-use residential, commercial, and administrative hubs, and sparsely populated newly created and peripheral areas (0–30 people/km²), dominated by newly developed estates and undeveloped land. This demographic and spatial duality shapes traffic patterns, with the city's road network - particularly King Abdulaziz Road - acting as a critical artery to accommodate both local commuter traffic and transnational freight. Stretching 3.7 km from south to north, King Abdulaziz Road connects Arar's historic downtown core to the Saudi-Iraq Highway (No. 80), a vital corridor for trade and cross-border movement and Highway 85 running from Saudi eastern region to Jordan border towards the West. The road's dual function as a commuter and freight corridor generates high daily traffic volumes, exacerbated by daily and seasonal peaks during holidays and trade cycles, while its aging infrastructure struggles to meet the demands of a growing vehicle fleet (Figure 1).

To analyze vehicular emissions under contrasting traffic regimes, two strategic monitoring points were selected along this corridor. The first is Point A, located at the southern entry point (30°58'09.4"N 41°00'55.1"E). It represents free-flow traffic conditions, where vehicles transition into the road at steady speeds with minimal interruptions, offering insights into baseline emissions during acceleration and cruising phases. The second survey Point B is a signalized intersection at the northern terminus (30°59'05.5"N 41°01'18.3"E). Point B experiences intermittent congestion due to merging traffic from secondary arterials, commercial zone access, and frequent stops at traffic signals, creating stop-and-go dynamics that amplify idling-related emissions. The selection of these points enables a granular comparison of emission profiles influenced by traffic behavior, steady-state driving versus stop-start conditions, while highlighting the impact of infrastructure design and traffic management on urban air quality. Furthermore, the study's findings

Figure 1. Study Area: location of the arterial King Abdulaziz Road and street view photo at peak evening hour using aerial satellite photos (© Google Maps)

hold relevance for mid-sized cities across the Gulf Cooperation Council (GCC) region facing similar challenges of rapid urbanization, traffic growth, and the need to align mobility policies with sustainability targets outlined in national agendas like Saudi Vision 2030 (Figure 2).

Data collection procedure

The data collection for traffic volume counts was conducted using a combination of automated sensors and observational tools tailored to the distinct traffic dynamics at the two monitoring points. At Point A (free-flow entry), Metrocount RoadPod 4 piezoelectric sensors were deployed to capture vehicle counts, speeds, and basic axle-based classification over a 72-hour period from Sunday, December 22, 2024, 11:00 AM to Wednesday, December 25, 2024, 11:00 AM. In contrast, Point B (signalized intersection) utilized a hybrid system integrating Metrocount sensors with camera-based systems (e.g., video analytics) to enable detailed vehicle classification (cars, trucks, buses, motorcycles) and real-time observation of traffic

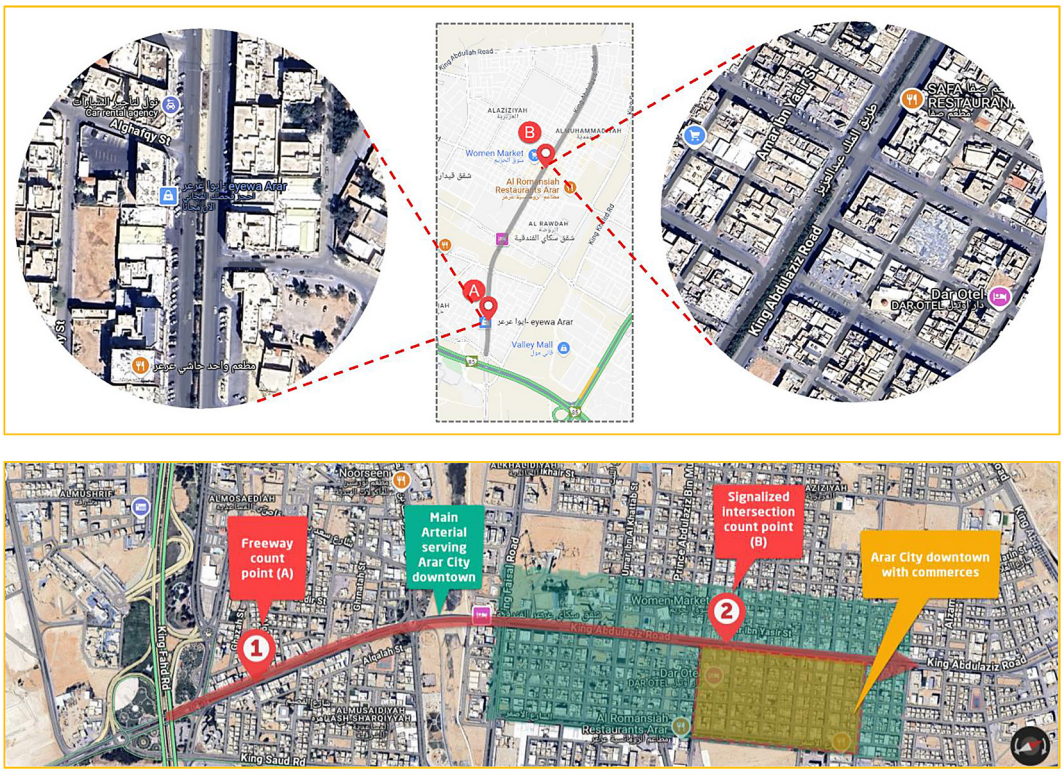

Figure 2. Locations of the traffic count points A (30°58’09.4”N 41°00’55.1”E) and B (30°59’05.5”N 41°01’18.3”E) using aerial satellite photos (© Google Maps)

behavior, such as idling duration and acceleration/deceleration patterns, over a longer 96-hour span from Wednesday, December 25, 2024, 11:00 AM to Sunday, December 29, 2024, 11:00 AM. Both datasets were structured into 15-minute temporal bins, aggregated into hourly intervals as per the "Weekly Vehicle Counts Report," and designed to capture variations across peak hours (7:00–9:00 AM, 5:00–7:00 PM), off-peak hours (12:00–3:00 PM, 10:00 PM–5:00 AM), and weekday/weekend cycles. Parameters included vehicle counts, classification, speed, and, for Point B, behavioral metrics critical for emission modeling under stop-and-go conditions. Data cleaning involved automated outlier removal (e.g., implausible speeds), calibration standardization between sensor types, and cross-validation of camera-based classifications against Metrocount axle data to ensure accuracy. Missing data gaps (<30 minutes) were filled via linear interpolation, while longer gaps were excluded. This multi-layered approach ensured high-resolution, context-specific insights into traffic dynamics, enabling robust emission estimation for contrasting flow regimes while addressing potential biases in sensor reliability and classification errors (Figure 3).

Vehicle emission estimation models

To estimate vehicular emissions along King Abdulaziz Road in Arar, this study employed gross emission models such as COPERT IV and MOVES, selected for their simplicity, scalability, and suitability for data-scarce regions. These models are widely used in urban planning and policy-making due to their reliance on readily available input data, such as traffic volume, vehicle classification, and average speeds, making them ideal for mid-sized cities like Arar, where detailed on-road emission measurements or advanced monitoring infrastructure may be limited. Emission factors, a cornerstone of these models, were adapted from peer-reviewed studies in similar Middle Eastern contexts to reflect local driving conditions and vehicle fleets. For instance, higher NO_x emission factors were assigned to diesel trucks, reflecting their disproportionate contribution to NO_x pollution, while CO spikes during idling at the signalized intersection (Point B) were explicitly accounted for. The calculation framework followed a standard gross emission formula:

$$Emission\left(\frac{g}{km}\right) = Traffic\,Volume \times \times Emission\,Factor \times Average\,Speed\,Adjustment \quad (1)$$

Where traffic volumes from Metrocount and camera-based systems were multiplied by pollutant-specific emission factors (differentiated by vehicle type) and adjusted for average speeds derived from observed driving patterns (e.g., stop-and-go delays at Point B). The analysis focused on four key pollutants: CO_2, a major greenhouse gas; CO, indicative of incomplete combustion; NO_x, linked to respiratory illnesses; and particulate matter (PM), a critical pollutant affecting air quality and public health. By integrating localized data with established modeling frameworks, this approach balances computational efficiency with contextual accuracy, providing actionable insights for urban areas facing rapid traffic growth and limited emission monitoring capabilities.

RESULTS AND DISCUSSION

Traffic volume

The two traffic count points (A and B) were strategically placed on the same arterial road to ensure full weekday coverage. Indeed, Point A covered Sunday to Wednesday. While Point B (located in Arar's core commercial area) spanned Wednesday to Sunday, capturing both weekdays and weekend days (Friday-Saturday in Saudi Arabia). This design ensures a representative sample of traffic patterns throughout the entire week and is suitable for a pilot study that will inform wider scope investigation (Figure 4).

The traffic volume data from Point A (free-flow entry) on King Abdulaziz Road in Arar reveals pronounced diurnal and weekly traffic patterns. It directly informs emission estimation dynamics. Morning rush hours (07:00–09:00) consistently recorded 539–593 vehicles/hour, peaking at 611 vehicles/hour on Wednesday (08:00–09:00), driven by commuter inflows into Arar's downtown core. Evening peaks (17:00–19:00) were even more intense, with 922–996 vehicles/hour, including 996 vehicles/hour on Tuesday (17:00–18:00), likely exacerbated by freight movements and post-work travel. These peaks highlight heightened emission risks from acceleration/deceleration cycles, despite free-flow conditions. Nighttime traffic (00:00–05:00) plummeted to 52–78 vehicles/hour, reflecting minimal

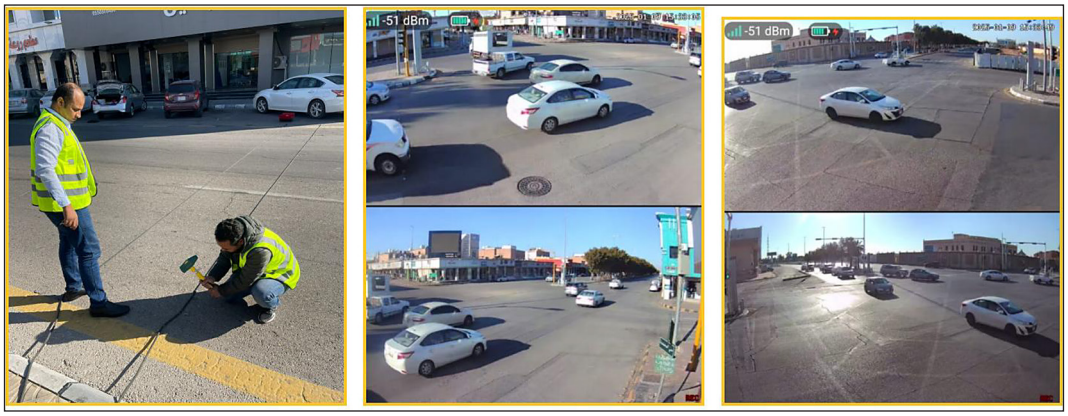

Figure 3. Field technicians deploying a hybrid traffic data collection system: Installation of MetroCount RoadPod VT4 pneumatic tubes for vehicle classification and counting, complemented by overhead camera monitoring for comprehensive intersection movement analysis and validation

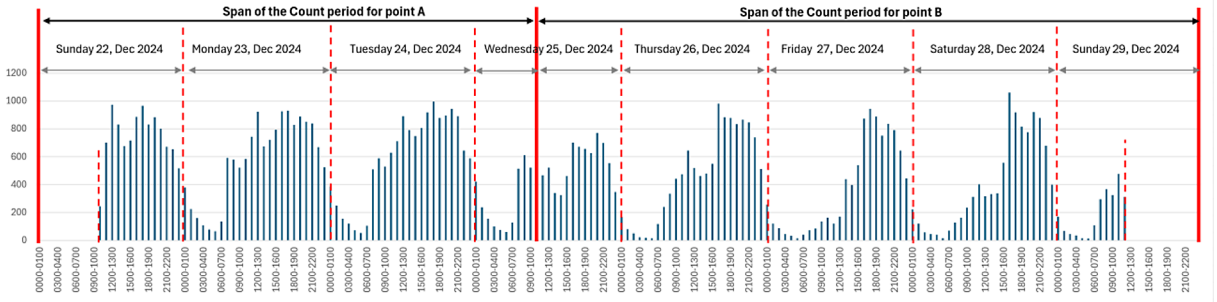

Figure 4. Periods of the traffic count showing temporal continuity and patterns similarity

nocturnal activity, while midday volumes (e.g., 922 vehicles/hour on Monday at 12:00–13:00) dipped on Tuesday (790 vehicles/hour), possibly due to reduced commercial activity or unrecorded disruptions (Figure 5).

Weekday traffic (Monday-Wednesday) maintained high daytime volumes (e.g., 8.817–8.997 vehicles/12 hours between 07:00–19:00). Sharp contrast was identified during weekends: Sunday saw 246–972 vehicles/hour, such as 246 vehicles/hour at 10:00–11:00, underscoring reduced economic and commuter activity on weekends. An anomalous Wednesday mid-morning drop (151 vehicles/hour, 10:00–11:00), compared to Monday's 743 vehicles/hour, suggests a potential sensor error or unrecorded event, though missing data for Thursday-Saturday limits full weekly trend validation. Despite gaps, weekday averages remain robust for modeling, emphasizing commuter and freight dominance in emission profiles. These findings underscore the necessity of hour-specific emission factors, as even free-flow corridors exhibit significant temporal variability, with peak-hour traffic disproportionately driving pollution. Targeted mitigation during evening rush hours and weekday planning could yield measurable air quality improvements in Arar's growing urban core.

The traffic volume data from Point B (signalized intersection) on King Abdulaziz Road in Arar highlights intense congestion and stop-and-go dynamics. This results in critical implications for emission hotspots. Morning rush hours (07:00–09:00) exhibited 765–854 vehicles/hour, peaking at 831 vehicles/hour on Sunday (13:00–14:00). This is driven by commuter inflows and merging traffic from secondary arterials. Evening peaks (17:00–19:00) were markedly higher, reaching 972 vehicles/hour on Sunday (18:00–19:00). this can be explained by vehicles queued at the signalized intersection created prolonged idling and acceleration/deceleration cycles. Unlike Point A's free-flow patterns, midday traffic at Point B remained elevated (702–972 vehicles/hour. Nighttime volumes (00:00–05:00) dropped sharply to 516–671 vehicles/hour, though still 10–20% higher than Point A due to residual freight traffic. Weekday vs. weekend comparisons revealed

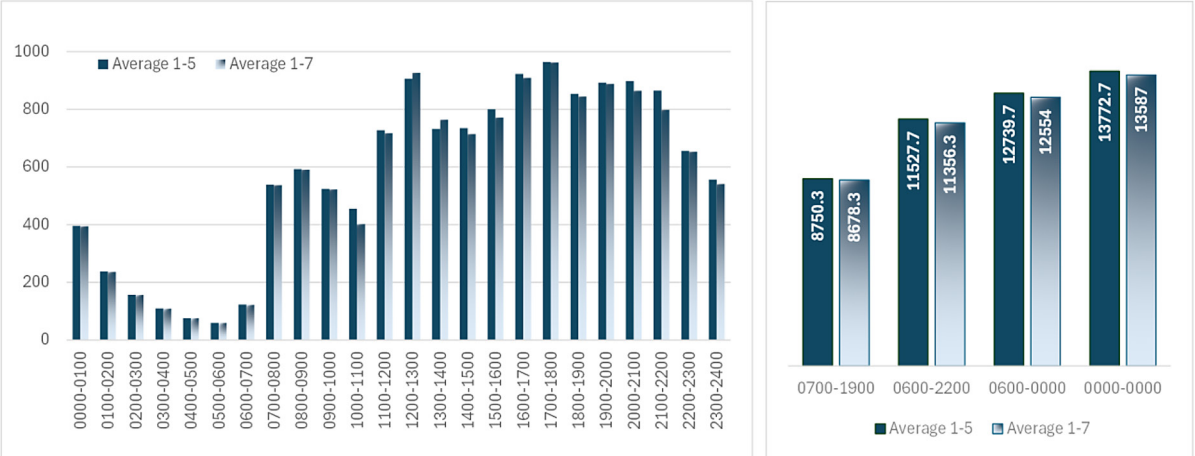

Figure 5. Traffic Counts at point A over a 72-hour period from Sunday, December 22, 2024, 11:00 AM to Wednesday, December 25, 2024, 11:00 AM

mixed trends: Monday-Wednesday saw steady peaks (e.g., 892–944 vehicles/hour at 20:00–21:00), while Saturday-Sunday showed 20–30% reductions during midday but sustained evening congestion (e.g., 884–965 vehicles/hour at 18:00–20:00), suggesting persistent freight and internal activity. Anomalies included a Wednesday midday spike (972 vehicles/hour, 12:00–13:00), possibly linked to signal timing adjustments, and a Thursday mid-afternoon dip (677 vehicles/hour, 14:00–15:00), potentially due to temporary roadworks. Missing data for Thursday-Saturday limit full trend analysis, but the observed patterns underscore Point B's role as a critical emission hotspot. The frequent idling and acceleration/deceleration cycles amplify CO and PM emissions despite similar weekday traffic volumes to Point A. These findings emphasize the need for intersection-specific mitigation strategies, such as adaptive signal control or low-idling zones, to address the disproportionate pollution generated in stop-and-go conditions (Figure 6).

The traffic and emission dynamics at Point A (free-flow entry) and Point B (signalized intersection) on King Abdulaziz Road in Arar reveal stark contrasts in urban mobility and pollution drivers. Point A exhibited moderate, commuter-dominated traffic with predictable morning (611 vehicles/hour) and evening (996 vehicles/hour) peaks, dropping sharply on weekends due to reduced residential activity. Emissions here were proportional to traffic volume, with NO_x and PM elevated during acceleration phases but lower CO spikes due to minimal idling. In contrast, Point B emerged as a congestion hotspot, with higher sustained volumes (peaking at 972 vehicles/hour) driven by merging freight, industrial traffic, and signal-induced stop-and-go cycles. Weekend activity at Point B declined less (20–30%) than Point A, underscoring its role in cross-border freight. Emissions here were disproportionately amplified: prolonged idling and frequent acceleration/deceleration cycles led to elevated CO and PM levels, even with similar weekday traffic volumes.

Traffic composition

Analysis of the traffic composition shows that both Point A and Point B are predominantly characterized by passenger vehicles (SV), accounting for approximately 94% of total traffic at each location (38,827 out of 41,164 at Point A and 36,511 out of 39,265 at Point B). The second most frequent vehicle type is 2-axle rigid trucks (TB2), with around 1.570 vehicles at both points. Notable differences between the points include higher motorcycle (MC) counts at Point B (101 vs 36) and a greater presence of 3-axle rigid trucks (T3) at Point B (404 vs 183). Heavy vehicle movements are also more frequent at Point B, as indicated by the higher numbers of 6-axle articulated trucks (ART6: 71 vs 33) and road trains (DRT: 49 vs 5). This suggests Point B may be more connected to freight routes while Point A appears to serve primarily urban passenger traffic (Figure 7) (Table 1).

The vehicle classification data from both survey points reveals a heavily passenger vehicle-dominated traffic composition. The Class 2 (standard passenger vehicles) comprises over 93% of all traffic at both locations. Point A shows 94.3% Class

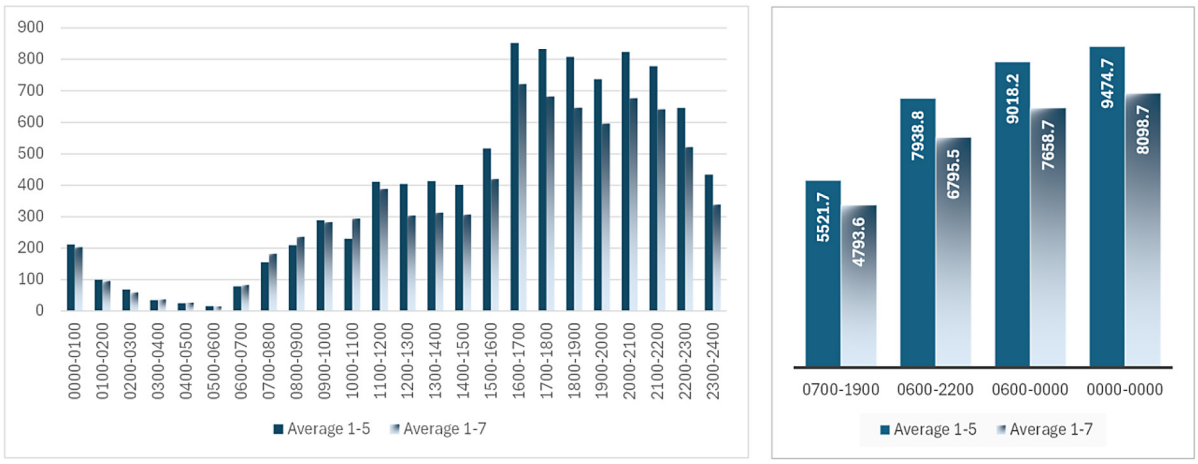

Figure 6. Traffic Counts at point B over a longer 96-hour span from Wednesday, December 25, 2024, 11:00 AM to Sunday, December 29, 2024, 11:00 AM

Table 1. Traffic composition at both Point A and Point B according to ARX classification for the full survey periods at point A and point B, Arar city

Point	Total	MC	SV	SVT	TB2	T3	T4	ART3	ART4	ART5	ART6	BD	DRT
Point A	41,164	36	38,827	211	1.576	183	57	16	193	25	33	2	5
Point B	39,265	101	36,511	238	1.570	404	81	23	190	20	71	7	49

Note: MC – Motorcycle, SV – Passenger Car, SVT – Car with Trailer, TB2 – 2 Axle Rigid Truck, T3 – 3 Axle Rigid Truck, T4 – 4 Axle Rigid Truck, ART3 – 3 Axle Articulated Truck, ART4 – 4 Axle Articulated Truck, ART5 – 5 Axle Articulated Truck, ART6 – 6 Axle Articulated Truck, BD – B-Double, DRT – Double/Road Train.

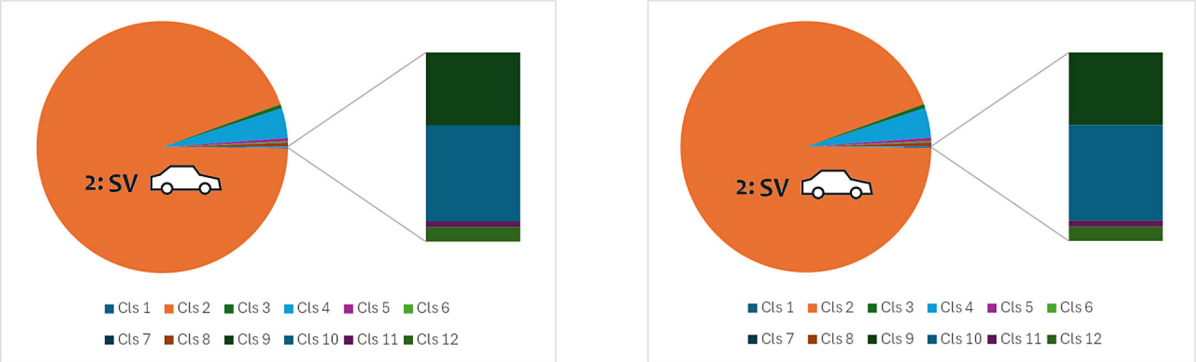

Figure 7. Distribution of vehicle classifications at Points A and B according to ARX classification system, showing predominance of Class 2 (passenger vehicles) at both locations

2 vehicles while Point B has 93%. The remaining distribution primarily consists of Class 4 vehicles (likely light commercial vehicles) at approximately 3.8–4% for both points. There are minimal differences between the two points. Indeed, Point B shows slightly higher percentages of Class 5 vehicles (1% vs 0.4%) and marginally higher representation of heavier vehicle classes. From an emissions perspective, this distribution suggests that passenger vehicle emission factors will dominate the overall emission inventory. The small but significant presence of commercial and heavier vehicles (Classes 4–12) should be accounted for as these vehicles typically have higher per-vehicle emission rates despite their lower numbers in the fleet.

Speed profiles

The speed distribution data from two monitoring points (A and B) shows a classical urban

traffic pattern with the majority of vehicles operating between 25–40 km/h. A peaking was recorded at 30–40 km/h for Point A (approximately 27%) and 25–30 km/h for Point B (about 26%). Point A demonstrates a slightly higher proportion of faster speeds (35–45 km/h) compared to Point B, while Point B shows higher percentages in lower speed ranges (10–25 km/h), suggesting different road or traffic conditions between the two locations. This speed distribution pattern has direct implications for vehicle emissions. Indeed, vehicles typically produce higher emissions during low-speed stop-and-go traffic (below 20 km/h) due to inefficient engine operation and frequent acceleration/deceleration cycles. The predominant mid-range speeds (25–40 km/h) generally represent more optimal operating conditions with lower per-kilometer emissions. This is though actual emission rates would also depend on other factors such as road grade, vehicle type, and driving behavior (Figure 8).

Emission factors

Emission factors in vehicle emission models are inherently complex due to their dependence on multiple variables including vehicle characteristics, driving conditions, meteorological factors, and fuel properties, making accurate estimation challenging (Zhong et al., 2024). To address uncertainties, researchers have employed various approaches such as Monte Carlo simulations (Lee and Park, 2024), sensitivity analyses (Chen et al., 2024), fuzzy logic methods (He et al., 2025), and probabilistic frameworks that incorporate confidence intervals and error propagation techniques. These uncertainty quantification methods help account for variabilities in input parameters, measurement errors, and model assumptions, though the complex interactions between factors like engine load, ambient temperature, vehicle maintenance, and driving behavior continue to present challenges in achieving high prediction accuracy across different operational scenarios.

Local meteorological conditions were incorporated to contextualize emission dispersion and vehicle performance. The climate features significant seasonal temperature variations, from winter lows of ~5 °C to summer highs of ~41 °C. These extremes directly influence emissions: colder temperatures increase cold-start emissions, while summer heat elevates loads from air conditioning use. Consequently, the emission adjustments implicitly account for these temperature-dependent effects. Furthermore, the wind regime is characterized by consistent north/northwesterly flows with moderate speeds (predominantly 20–30 km/h), which governs the predominant downwind dispersion of pollutants. This wind pattern was considered in interpreting the spatial impact of emissions but was not used to adjust the emission factors themselves (Figure 9).

The estimation of vehicle emissions in this research relies on established emission factors (EFs) derived from existing literature (Gao et al., 2022; Perdikopoulos et al., 2025; Sirithian et al., 2022), COPERT, MOVES regulatory models (Liu et al., 2023; Sun et al., 2023; Xu et al., 2023) and published research work data (Ye et al., 2025). While these values serve as reference points for illustrative purposes, they may not fully capture the unique characteristics of

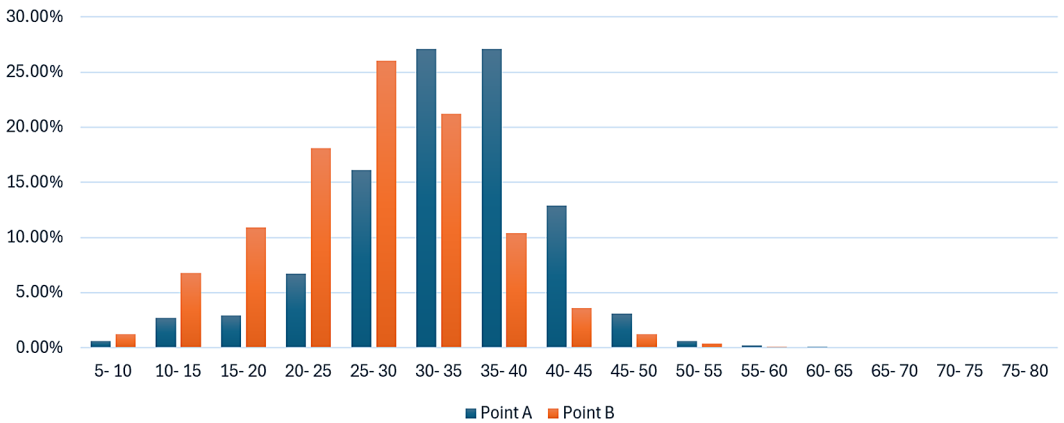

Figure 8. Vehicle speed distribution comparison between Point A and Point B, showing percentage frequency across speed ranges from 5 to 80 km/h

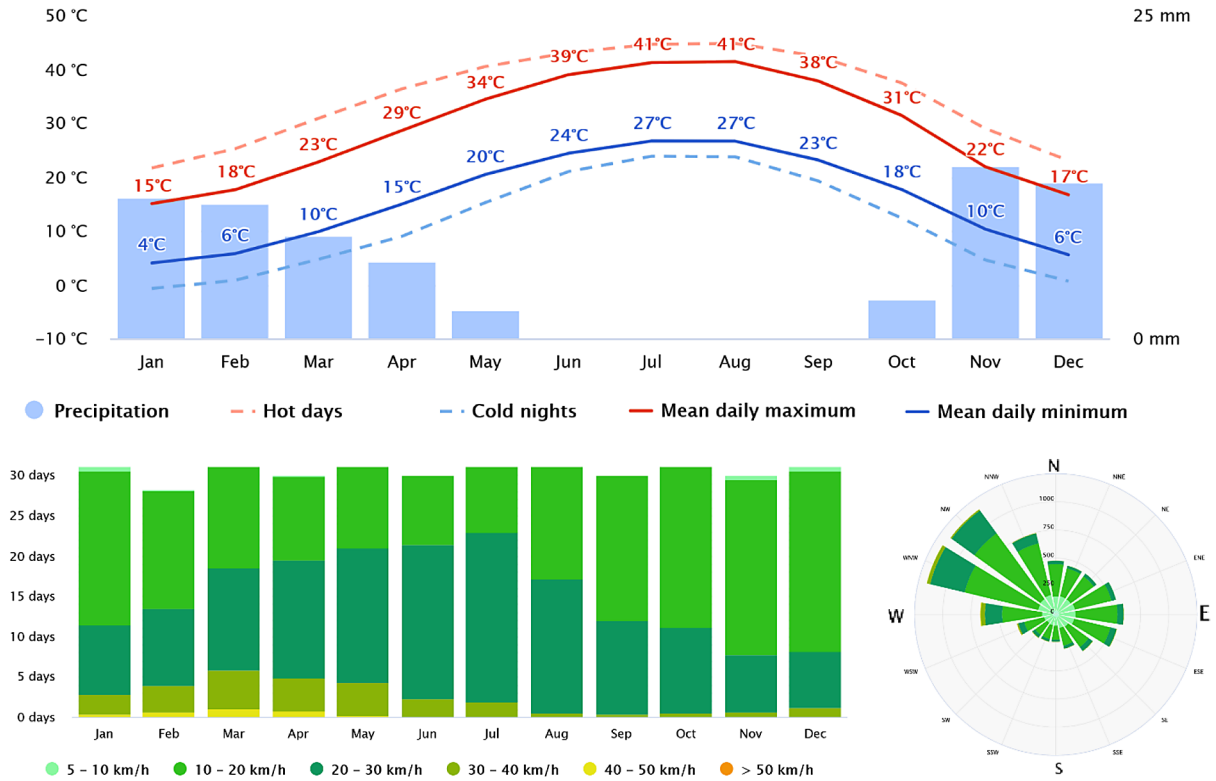

Figure 9. (a) Annual temperature regime showing mean daily maximum and minimum temperatures, hot days, cold nights, and precipitation patterns at the study area. Annual wind regime displaying monthly wind speed distribution (stacked bars, left) and directional frequency (wind rose, right) at the study area. (b) Wind speeds categorized in ranges from 5–10 km/h to >50 km/h. Data source: MeteoBlue

Saudi Arabia's context. Site-specific calibration studies are essential for medium and large Saudi cities, considering the region's distinctive climatic conditions, fleet composition, emission regulations, and other local parameters that significantly influence emission patterns. Future research should prioritize comprehensive field measurements to develop and validate emission prediction models that accurately reflect Saudi Arabia's transportation ecosystem.

The application of emission factors in this study incorporated adjustments for key regional characteristics, namely fuel standards, high ambient temperatures, and an aged vehicle fleet, through specific uplift factors. It is critical to note, however, that these adjustments introduce a significant layer of uncertainty, as the chosen uplifts (+15% for passenger cars, +12% for light commercial veicles, +10% for trucks, and +8% for buses) are expert estimates based on a qualitative synthesis of literature rather than locally validated coefficients. Consequently, while this approach provides a necessary first-order approximation for the Saudi context, the resulting emission estimates are inherently uncertain. This primary uncertainty, stemming from the use of non-localized emission factors, is compounded by other limitations including the temporal representativeness of traffic data, the documented accuracy margins of the $PM_{2.5}$ sensors, and the use of typical rather than highly resolved meteorological data in dispersion modeling (Table 2).

Emission estimates

The traffic composition analysis reveals a predominantly passenger car-oriented traffic flow, with passenger vehicles constituting approximately 94% (Point A) and 93% (Point B) of total daily traffic. Light commercial vehicles form the second largest category at about 4–5% of total flow, while heavy-duty trucks represent only 1–2% of traffic volume. The notably low bus traffic (less than 0.1% at Point A and 0.14% at Point B) suggests limited public transport service in the surveyed area. Point A experiences higher overall traffic volumes with 13,720 vehicles per day compared to Point B's 9.818, though Point B

Table 2. Emission factors used to estimate the vehicle emission estimates from the traffic data at Arar city

Vehicle Category	Scenario	CO_2	CO	NO_x	$PM_2.5$
Passenger Cars (Class 2)	Baseline (Publication-Regulations)	170–180	1.10–1.20	0.20–0.25	0.004–0.005
	Adjusted - Saudi Arabia	195	1.38	0.29	0.006
Light Commercial (Class 3-4)	Baseline (Publication-Regulations)	210–225	1.50–1.60	0.30–0.35	0.009–0.010
	Adjusted - Saudi Arabia	235	1.68	0.34	0.011
Heavy-Duty Trucks (Class 5-8)	Baseline (Publication-Regulations)	600–650	3.80–4.00	3.80–4.20	0.045–0.050
	Adjusted - Saudi Arabia	660	4.20	4.18	0.055
Buses (Class 9-12)	Baseline (Publication-Regulations)	870–920	4.70–5.00	4.60–5.00	0.070–0.080
	Adjusted - Saudi Arabia	940	5.10	5.00	0.086

shows slightly higher proportions of heavy vehicles and buses, possibly indicating different land use patterns or route preferences for commercial traffic. The distribution of the ADT by vehicle category is obtained and provided (The translation of aggregated traffic counts (Table 1) to Average Daily Traffic (ADT) data yields:

- Point A: ADT = Total count / (72/24) = 41,164 / 3 = 13,721 vehicles/day
- Point B: ADT = Total count / (96/24) = 39,265 / 4 = 9.816 vehicles/day (Table 3)

The translation of aggregated traffic counts (Table 1) to average daily traffic (ADT) data yields:

- Point A: ADT = Total count / (72/24) = 41,164 / 3 = 13,721 vehicles/day
- Point B: ADT = Total count / (96/24) = 39,265 / 4 = 9.816 vehicles/day

Furthermore, the daily average traffic speeds are computed using the speed matrix for the survey point A and B. For illustrative purposes, the computation details at the signalized intersection are presented below and summarized in Table 4:

- Passenger Cars (Class 2) = SV only: Weighted average = 44.1 km/h
- Light Commercial (Class 3–4) = SVT + TB2: Weighted average = 41.5 km/h
- Heavy-Duty Trucks (Class 5–8) = TB3 + T4 + ART3 + ART4: Weighted average = 29.9 km/h
- Buses (Class 9–12) = ART5 + ART6 + BD + DRT: Weighted average = 35.9 km/h

The daily average speed data (Table 4) shows consistently higher speeds at Point A across all vehicle categories, with the most pronounced difference observed in heavy-duty trucks (19.7 km/h faster at Point A). Other vehicle categories show speed differences of 9–11 km/h, suggesting significantly better traffic flow conditions at Point A compared to Point B.

In mileage-based vehicle emission estimation models, the emission factors increase outside an optimal speed range characteristic of the vehicle category. To account for speed variability impact on emissions, Table 4 presents speed correction factors (SCFs) provided based on the optimal range of each vehicle category:

- Passenger cars: Optimal range centered around 60 km/h for urban arterials
- Light commercial: Slightly lower optimal range due to vehicle weight/mechanics
- Heavy trucks/buses: Lower optimal range considering vehicle dynamics and urban operations

The SCFs show moderate corrections needed at Point A where speeds are close to optimal ranges. Point B still requires higher corrections, especially for heavy vehicles, but the factors are more aligned with real-world vehicle performance characteristics.

For the survey point B as an example, the results yield a typical speed hierarchy: passenger cars operating at the highest speeds (44.1 km/h), followed by light commercial vehicles (41.5 km/h), buses (35.9 km/h), and heavy-duty trucks maintaining the lowest average speeds (29.9 km/h), which better reflects typical urban traffic patterns and vehicle operational characteristics. Using a unit traveled distance, Vehicle Kilometers Traveled (VKT) is calculated using the equation below (Ishak et al., 2022; Mun and Jung, 2025; Park and Park, 2024; Patiño-Aroca et al., 2022) and summarized in Table 5.

$$VKT = Number\ of\ vehicles \times \times Road\ segment\ length\ (km) \quad (2)$$

To compute the estimates of emissions induced by the traffic at selected count points, the results are consolidated using the previous results presented in Table 2, Table 4, Table 5 and Table 6.

Table 3. Average daily traffic (ADT) Distribution by vehicle category at two major survey points in Arar City, Saudi Arabia

Vehicle Category	Survey Point A Count (24h)	Survey Point B Count (24h)
Passenger Cars (Class 2)	12,954	9.153
Light Commercial (Class 3-4)	595	453
Heavy-Duty Trucks (Class 5-8)	168	198
Buses (Class 9-12)	3	14
Total	13,720	9.818

Table 4. Daily average traffic speeds by vehicle category at survey points A and B in Arar City with speed correction factors (SCFs)

Vehicle category	Daily average speed (km/h)			Speed correction factor (SCF)		
	Point A	Point B	(A-B)	Optimal range	Point A	Point B
Passenger cars	53.4	44.1	+9.3	50–70 km/h	1.12	1.25
Light commercial	51.0	41.5	+9.5	45–65 km/h	1.08	1.20
Heavy-duty trucks	49.6	29.9	+19.7	40–60 km/h	1.01	1.50
Buses	46.5	35.9	+10.6	40–60 km/h	1.08	1.40

Carbon dioxide (CO_2)

CO_2 emissions demonstrate strong correlation with traffic volume and vehicle type distribution, showing distinct patterns at both survey points. At Point A, passenger cars are the dominant contributors (2.83M g/day/km), reflecting the high traffic volume (12,954 vehicles) and moderate speeds (53.4 km/h). Despite lower traffic volumes at Point B (9.153 passenger cars), the reduced speeds (44.1 km/h) result in disproportionately high emissions (2.23M g/day/km). Heavy trucks show an inverse pattern, with Point B emissions (196,614 g/day/km) significantly exceeding Point A (112,277 g/day/km) despite similar vehicle counts, primarily due to the speed differential (29.9 vs 49.6 km/h). Saudi Arabian factors consistently yield 15–20% higher CO_2 emissions compared to baseline scenarios, reflecting local fleet characteristics and operating conditions.

Carbon monoxide (CO)

CO emissions follow patterns similar to CO_2 but with more pronounced variations between vehicle categories and locations. Passenger cars at Point A emit 20,034 g/day/km compared to 15,789 g/day/km at Point B, representing a smaller proportional difference than CO_2. Heavy vehicles show particularly sensitive CO emission responses to speed variations, with Point B's lower speeds resulting in notably higher emissions per vehicle. The - scenarios show 20–25% increases over baseline values, suggesting that local conditions significantly impact incomplete combustion processes that generate CO. The relationship

Table 5. Average daily traffic (ADT) distribution by vehicle category at two major survey points in Arar City, Saudi Arabia

Category	Survey Point A			Survey Point B		
	Count (24h)	Average Speed (km/h)	VKT (Count × Length)	Count (24h)	Average Speed (km/h)	VKT (Count × Length)
Passenger Cars (Class 2)	12,954	53.4	12,954	9.153	44.1	9.153
Light Commercial (Class 3–4)	595	51.0	595	453	41.5	453
Heavy-Duty Trucks (Class 5–8)	168	49.6	168	198	29.9	198
Heavy-Duty Trucks (Class 5–8)	3	46.5	3	14	35.9	14
Total	13,720		13,720	9.818		9.818

Table 6. Estimated emissions at survey point A and point B (g/day/km)

Category	Scenario	Survey Point A				Survey Point B			
		CO_2	CO	NOx	PM2.5	CO_2	CO	NOx	PM2.5
Passenger Cars	Baseline Low	2,466,726	15,997	2.908	58.2	1,943,516	12,604	2,291	45.8
	Baseline High	2,611,712	17,451	3.635	72.7	2,057,430	13,750	2,863	57.2
	Adjusted SA	2,830,305	20,034	4.210	87.1	2,232,206	15,789	3,318	68.6
Light Commercial	Baseline Low	134,865	963	193	5.8	114,156	815	163	4.9
	Baseline High	144,498	1.027	225	6.4	122,310	869	190	5.4
	Adjusted SA	150,754	1.079	218	7.1	127,674	914	185	6.0
Heavy Trucks	Baseline Low	101,808	644	644	7.6	178,200	1.128	1,128	13.4
	Baseline High	110,292	678	713	8.5	193,050	1.188	1.247	14.9
	Adjusted SA	112,277	714	711	9.4	196,614	1.250	1.245	16.4
Buses	Baseline Low	2,808	15.2	14.9	0.23	17,052	92.3	90.2	1.37
	Baseline High	2,970	16.1	16.1	0.26	18,032	98.0	98.0	1.57
	Adjusted SA	3,052	16.6	16.2	0.28	18,532	100.5	98.4	1.69

between speed and CO emissions appears more complex than for CO_2, particularly in the heavy vehicle categories.

Nitrogen oxides (NOx)

NOx emissions exhibit the most dramatic variations among pollutants, particularly for heavy vehicles. The - scenarios show substantial increases over baseline values (25–30%), reflecting the sensitivity of NOx formation to local operating conditions. At Point B, heavy truck NOx emissions (1.245 g/day/km) are significantly higher than at Point A (711 g/day/km), despite similar vehicle counts, demonstrating the critical impact of speed on NOx formation. Passenger car NOx emissions show less dramatic but still significant variations between points (4.210 vs 3.318 g/day/km), suggesting that light vehicle NOx emissions are less sensitive to speed variations than heavy vehicles.

Particulate matter (PM2.5)

PM2.5 emissions show the highest relative increases in adjusted scenarios compared to baseline values, particularly for heavy vehicles. The speed impact is most pronounced in this pollutant, with Point B's lower speeds resulting in significantly higher per-vehicle emissions, especially for heavy trucks (16.4 vs 9.4 g/day/km). Passenger car PM2.5 emissions demonstrate notable differences between points (87.1 vs 68.6 g/day/km). However, the relative impact of speed is less influencial than for heavy vehicles. The results suggest that PM2.5 emissions are particularly sensitive to both vehicle type and operating conditions, with implications for air quality management strategies in urban areas.

CONCLUSIONS

This study quantified traffic-induced emissions at a free-flow corridor (Point A) and a signalized corridor (Point B) in Arar city, Saudi Arabia, by combining one-week, 1-h traffic counts with locally-adjusted emission factors. Despite comparable daily traffic volumes, the presence of signal control fundamentally altered the emissions profile. At Point B, extended idling and repetitive acceleration/deceleration cycles during the morning (07:00–09:00) and evening (17:00–19:00) peaks elevated corridor-average CO and $PM_{2.5}$ by 65–75% relative to Point A. These findings corroborate earlier micro-scale analyses that identify queuing as a primary determinant of urban roadside pollution rather than absolute vehicle counts.

Although passenger cars constituted more than 93% of the fleet at both sites, a small cohort of heavy-duty trucks (smaller than 7% by number) proved responsible for a disproportionate share of regulated pollutants. At Point B, trucks contributed 1 245 g/day/km of NO_x and 16.4 g/day/km of $PM_{2.5}$, values 75% and 74% higher, respectively, than those observed at the free-flow site. The effect was amplified by mean truck speeds of only 29.9 km/h, well below the threshold at which diesel after-treatment systems operate efficiently. These results confirm that targeted abatement of the heavy-duty segment can yield

outsized air-quality benefits, even in passenger-car-dominated traffic streams.

Application of Saudi-specific uplifts (+15% for light-duty and +10–12% for heavy-duty vehicles) raised default COPERT/MOVES baseline CO_2 emissions by up to 20% and NO_x by up to 30%. The magnitude of this adjustment underscores the necessity of regional calibration when transferring emission factors from temperate, high-income contexts to arid, high-temperature environments. Nonetheless, the absence of chassis-dynamometer or PEMS validation data for the local fleet remains a critical source of uncertainty.

From a management perspective, the results advocate site-specific interventions rather than city-wide blanket measures. Adaptive signal control, dynamic peak-hour freight restrictions, and enforcement of Euro 6/VI standards for trucks at Point B are expected to reduce corridor-level $PM_{2.5}$ by ~20% and NO_x by ~25% under conservative uptake scenarios. Moreover, the high temporal resolution of the MetroCount data set facilitates the design of demand-responsive pricing schemes or real-time driver information systems that smooth peak flows and restore average speeds above 50 km/h.

The analysis is constrained by three principal limitations: (i) missing weekend data (Thursday–Saturday) precluded full characterization of weekly variability; (ii) the emission model did not explicitly incorporate meteorology, road gradient, or cold-start effects; and (iii) Saudi-specific adjustment factors were inferred rather than empirically derived. Future work should therefore extend temporal coverage, integrate IoT-based meteorological and exhaust sensors for online calibration, and employ dispersion modelling to link roadside emissions with population exposure.

In summary, the interaction of congestion dynamics and a minor heavy-duty sub-fleet defines the dominant urban emission hotspots in Arar. The study demonstrates that granular traffic monitoring, coupled with regionally adapted emission factors, can generate actionable insights for near-term air-quality improvement in rapidly motorizing Middle-Eastern cities.

Acknowledgements

The authors extend their appreciation to the Deanship of Scientific Research at Northern Border University, Arar, KSA for funding this research work through the project number NBU-FFR-2025-2122-02. The author also extends his thanks to Waleed Engineering Consultant Office (WECO) for the enabling and making available the data for the research.

REFERENCES

1. Adresi, M., Abedi, M., Dong, W., Yekrangnia, M. (2024). A review of different types of weigh-in-motion sensors: State-of-the-art. *Measurement*, *225*, 114042.
2. Ansariyar, A., Taherpour, A., Yang, D., Jeihani, M. (2024). Comparative analysis of LiDAR and CCTV sensor accuracy at signalized intersections under varied weather conditions. *International Journal of Transport Development and Integration*, *8*(2). https://trid.trb.org/View/2417261
3. Chen, J., Yu, H., Xu, H., Lv, Q., Zhu, Z., Chen, H., Zhao, F., Yu, W. (2024). Investigation on traffic carbon emission factor based on sensitivity and uncertainty analysis. *Energies*, *17*(7), 1774.
4. Cherif, B., Ghazzai, H., Alsharoa, A., Besbes, H., Massoud, Y. (2023). Aerial LiDAR-based 3D Object Detection and Tracking for Traffic Monitoring. *2023 IEEE International Symposium on Circuits and Systems (ISCAS)*, 1–5. https://doi.org/10.1109/ISCAS46773.2023.10181371
5. Fathima, M. D., Hariharan, R., C, G., S, E. R. (2025). Smart Street: AI-Powered Traffic Flow Enhancement with Adaptive Signal Control. In A. Verma, P. Verma, K. K. Pattanaik, R. Buyya, D. Dasgupta (Eds.), *Advanced Network Technologies and Intelligent Computing* 144–158. Springer Nature Switzerland. https://doi.org/10.1007/978-3-031-83796-8_10
6. Gao, C., You, H., Gao, C., Na, H., Xu, Q., Li, X., Liu, H. (2022). Analysis of passenger vehicle pollutant emission factor based on on-board measurement. *Atmospheric Pollution Research*, *13*(6), 101421. https://doi.org/10.1016/j.apr.2022.101421
7. Gautam, V., Sunidhi, S., Prasad, S. (2025). AI-Powered Surveillance for Smart Cities. In A. Abraham, S. Prasad, A. Alhammadi, T. Lestable, F. Chaabane (Eds.), *Internet of Vehicles and Computer Vision Solutions for Smart City Transformations* 245–265. Springer Nature Switzerland. https://doi.org/10.1007/978-3-031-72959-1_11
8. Giechaskiel, B., Casadei, S., Rossi, T., Forloni, F., Di Domenico, A. (2021). Measurements of the emissions of a "golden" vehicle at seven laboratories with portable emission measurement systems (PEMS). *Sustainability*, *13*(16), Article 16. https://doi.org/10.3390/su13168762
9. Guan, F., Xu, H., Tian, Y. (2023). Evaluation of roadside LiDAR-based and vision-based multi-model all-traffic trajectory data. *Sensors*, *23*(12), 5377.

10. Gurung, P. (2025). Drone-assisted imaging and vehicle telemetry integration for enhanced smart mobility applications. *Reviews on Internet of Things (IoT), Cyber-Physical Systems, and Applications*, *10*(1), Article 1.
11. He, S., Lin, Y., Wei, Z., Wan, M., Min, Y. (2025). Sustainable emission control in heavy-duty diesel trucks: fuzzy-logic-based multi-source diagnostic approach. *Sustainability*, *17*(8), Article 8. https://doi.org/10.3390/su17083605
12. Ishak, S. Z., Ibrahim, N. A. S., Kamaluddin, N. A., Dhokhikah, Y. (2022). Vehicle kilometers traveled (VKT) for campus population: case study of UiTM main campus. *Environment-Behaviour Proceedings Journal*, *7*(SI9), Article SI9. https://doi.org/10.21834/ebpj.v7iSI9.4315
13. Kawsar, S., Biswas, S., Noor, M., Mamun, M. S. (2024). Investigating the applicability of COPERT 5.5 emission software in Bangladesh and developing countrywide vehicular emission inventories. *Environmental Science: Atmospheres*, *4*(1), 57–72.
14. Lee, M. H., Park, Y.-K. (2024). Emission factor estimation using monte carlo simulation: focusing on the development of dioxin emission factors in cremation facilities. *Korean Journal of Chemical Engineering*, *41*(9), 2607–2619. https://doi.org/10.1007/s11814-024-00211-4
15. Li, S., Du, Y. (Eliza), Jiang, Y. (2010). Site verification of weigh-in-motion traffic and TIRTL classification data. *JTRP Technical Reports*. https://doi.org/10.5703/1288284314247
16. Liu, R., He, H., Zhang, Z., Wu, C., Yang, J., Zhu, X., Peng, Z. (2023). Integrated MOVES model and machine learning method for prediction of CO_2 and NO from light-duty gasoline vehicle. *Journal of Cleaner Production*, *422*, 138612. https://doi.org/10.1016/j.jclepro.2023.138612
17. Mararo, L. E., Gariy, A., Jospha, M. (2015). A macroscopic fundamental diagram for spatial analysis of traffic flow: A case study of Nyeri Town, Kenya. *Am. J. Civ. Eng*, *3*, 150–156.
18. Matsuoka, M., Hirai, H., Ito, T. (2025). *Evaluation of Portable Emission Measurement Systems (PEMS) Accuracy by Simultaneous Measurement of PEMS and Laboratory-Based Analyzers** (SAE Technical Paper Nos. 2024-32–0113). SAE International. https://doi.org/10.4271/2024-32-0113
19. Mun, H., Jung, J. (2025). Relationships between vehicle kilometers traveled and carbon emissions based on urban size. *KSCE Journal of Civil Engineering*, *29*(6), 100112. https://doi.org/10.1016/j.kscej.2024.100112
20. N, B., S, P., K, K. V. (2023). AI-powered Traffic Lights. *2023 Intelligent Computing and Control for Engineering and Business Systems (ICCEBS)*, 1–5. https://doi.org/10.1109/ICCEBS58601.2023.10449105
21. Park, J., Park, S. (2024). Estimating regional CO_2 and NOx emissions from road transport using real-world data-based emission factors in Korea. *Environmental Pollution*, *352*, 124140. https://doi.org/10.1016/j.envpol.2024.124140
22. Patiño-Aroca, M., Parra, A., Borge, R. (2022). On-road vehicle emission inventory and its spatial and temporal distribution in the city of Guayaquil, Ecuador. *Science of The Total Environment*, *848*, 157664. https://doi.org/10.1016/j.scitotenv.2022.157664
23. Peppa, M. V., Komar, T., Xiao, W., James, P., Robson, C., Xing, J., Barr, S. (2021). Towards an end-to-end framework of CCTV-based urban traffic volume detection and prediction. *Sensors*, *21*(2), 629.
24. Perdikopoulos, M., Karageorgiou, T., Ntziachristos, L., Deville Cavellin, L., Joly, F., Vigneron, J., Arfire, A., Debert, C., Sanchez, O., Gaie-Levrel, F., Marfaing, H. (2025). Developing emission factors from real-world emissions of Euro VI urban diesel, diesel-hybrid, and compressed natural gas buses. *Atmosphere*, *16*(3), Article 3. https://doi.org/10.3390/atmos16030293
25. Piotrowicz, A., Polednik, B. (2019). Exposure to Aerosols particles on an urban road. *Journal of Ecological Engineering*, *20*(5), 27–34. https://doi.org/10.12911/22998993/105329
26. Rymaniak, Ł., Mąka, M., Szymlet, N., Kamińska, M., Kęska, A. (2023). Measurement of exhaust emissions from a two-wheeler – an experimental validation of the remote-sensing method. *Journal of Ecological Engineering*, *24*(12), 60–71. https://doi.org/10.12911/22998993/171900
27. Saberiyansani, M., Rashidi, Y., Hashemi, S. H. (2025). Comparative analysis of COPERT and IVE models in road transport emission assessment. *Sustainable Earth Trends*, *5*(3). https://search.ebscohost.com/login.aspx?direct=true&profile=ehost&scope=site&authtype=crawler&jrnl=30606225&AN=184592068&h=52c8kSIwQqzpscS%2Fyb3Vj2DpeEWp3GhbW3dCuDCPkMYN7rKWPgBNpQ3sMoaGY5HcuBsB9luo4z6fnpDUkftAhw%3D%3D&crl=c
28. Segarra-Morales, S., Moreno, A. T. (2024). A Comparative Study of Speed Measurement Using Radar Guns and Pneumatic Counter. In K. Daimi & A. Al Sadoon (Eds.), *Proceedings of the Third International Conference on Innovations in Computing Research (ICR'24)* 204–212. Springer Nature Switzerland. https://doi.org/10.1007/978-3-031-65522-7_19
29. Sirithian, D., Thanatrakolsri, P., Pongpan, S. (2022). CO_2 and CH_4 emission factors from light-duty vehicles by fuel types in Thailand. *Atmosphere*, *13*(10), Article 10. https://doi.org/10.3390/atmos13101588
30. Sun, Y., Hu, Y., Zhang, H., Chen, H., Wang, F.-Y. (2023). A parallel emission regulatory framework for intelligent transportation systems and

smart cities. *IEEE Transactions on Intelligent Vehicles*, *8*(2), 1017–1020. https://doi.org/10.1109/TIV.2023.3246045

31. US EPA, O. (2016, January 12). *Global Greenhouse Gas Overview* [Overviews and Fact-sheets]. https://www.epa.gov/ghgemissions/global-greenhouse-gas-overview
32. vizen. (2025, April 7). Global anthropogenic nitrogen dioxide emissions, 1750-2022. *Visualizing Energy*. https://visualizingenergy.org/global-anthropogenic-nitrogen-dioxide-emissions-1750-2022/
33. Wei, P., Brimblecombe, P., Yang, F., Anand, A., Xing, Y., Sun, L., Sun, Y., Chu, M., Ning, Z. (2021). Determination of local traffic emission and non-local background source contribution to on-road air pollution using fixed-route mobile air sensor network. *Environmental Pollution*, *290*, 118055. https://doi.org/10.1016/j.envpol.2021.118055
34. Xu, Z., Kang, Y., Cao, Y., Li, Z. (2021). Deep amended COPERT model for regional vehicle emission prediction. *Science China. Information Sciences*, *64*(3), 139202.
35. Xu, Z., Wang, R., Pan, K., Li, J., Wu, Q. (2023). Two-stream networks for COPERT correction model with time-frequency features fusion. *Atmosphere*, *14*(12), Article 12. https://doi.org/10.3390/atmos14121766
36. Ye, H., Li, Y., Zheng, J., Li, Z. (2025). City-level estimation of vehicle CO2 emission factors regarding driving behaviors: The case of Tianjin, China. *Heliyon*, *11*(1). https://doi.org/10.1016/j.heliyon.2024.e41253
37. Zhong, H., Chen, K., Liu, C., Zhu, M., Ke, R. (2024). Models for predicting vehicle emissions: A comprehensive review. *Science of The Total Environment*, *923*, 171324. https://doi.org/10.1016/j.scitotenv.2024.171324